

THE CONFORMAL CAMERA IN MODELING VISUAL INFORMATION DURING EYES MOVEMENTS

Jacek Turski

Department of Computer and Mathematical Sciences, University of Houston-Downtown, One Main Street, Houston, U.S.A.

Keywords: The conformal camera, Projective Fourier transform, Retinotopy, Saccades, Perisaccadic perception, Pursuit.

Abstract: The conformal camera and its related projective Fourier transform that provide image representation well adapted to projective transformations and retinotopic mappings of the brain visual pathways are reviewed. The conformal camera's non-Euclidean geometry effectiveness in intermediate-level vision is discussed, the algorithmic steps in modeling visual information during saccadic eye movements are outlined, and the research-in-progress on modeling perception during pursuit eye movements is described. It is concluded that the conformal camera may provide a computational framework needed for developing tools for processing visual information during the exploratory movements of the camera with a silicon retina, used in autonomous mobile robots.

1 INTRODUCTION

The light carrying visual information about the external world enters the primate vision system through the eyeball pupil, strikes photoreceptors where the transduction into electrical impulses takes place, and passes through the multi-layered neuronal circuitry of the retina where it undergoes initial processing. The retinal output is conveyed to numerous downstream brain areas for further processing, and, when combined with other sensory information, results in our understanding of the 3D world that guides our actions.

This problem, which the brain must solve in real-time, is immensely complex. One of the reasons for complexity is the fact that primates see clearly only the central two degrees of the visual field projected on the central fovea consisting mainly of a high density cone cells, the color-selective type of photoreceptors for a sharp daylight vision. The visual acuity decreases rapidly away from the fovea because the distance between cones increases with eccentricity as they are outnumbered by rod cells, photoreceptors for a low acuity black-and-white night vision. Moreover, there is an increased convergence of the photoreceptors on the ganglion cells whose axons send out retinal information to the brain areas in precise retinotopic arrangements. To overcome this acuity limitation, the brain executes a scanning eye movement consisting of a sequence of saccades that reposition the fovea on the objects of interest, interlaced with fixations, during which, the visual information is acquired. Usually humans make about three sac-

cadés per second at the eyeball's maximum speed of 700 deg/sec, producing about 200,000 saccades per day. This sequence of saccades, fixations, and, sometimes also smooth-pursuit eye movements that keep the fovea focused on a slowly (up to 100 deg/sec) moving object for detailed analysis, is the most basic feature underpinning primate visual perception.

Although, there has been great progress made in understanding the neural processes underlying our clear and stable perception in spite of limited acuity and incessant eye movements, see (Klier and Angelaki, 2008; Wurtz, 2008) for reviews, the involved mechanisms are still not fully understood. Converging evidence from psychophysics, functional neuroimaging, and primate neurophysiology supports the current view that the most attractive neural basis that underlies visual stability are the mechanisms partially suppressing visual sensitivity during saccades and causing visual and visuo-motor cells in various brain areas to respond to stimuli before the eyes move their receptive fields there, commonly referred to as the shifting receptive fields mechanism (Duhamel et al., 1992; Melcher and Colby, 2007). This shift of receptive fields, starting 50 ms before a saccade onset and ending 50 ms after the saccade landing, is hypothesized to update (or remap) the retinotopic maps in the anticipation of each upcoming saccade.

From the above review of visual neuroscience, one should not be surprised that, in spite of the sustained efforts over many decades that have resulted in significant advances in the application of robotics to industry, medicine, the military, space and under-

water explorations, humanoid robots are still far in the future. On the other hand, with the recent proposed research program on trans-saccadic perception (Melcher and Colby, 2007), it is becoming now important to propose biologically-mediated engineering approaches in modeling visual information during the exploratory eye movements. This has been the main goal of our recent work (Turski, 2010) which we review in this article.

We model the eyes' imaging functions with the conformal camera we have developed for robotic vision. Remarkably, the conformal camera possesses its own projective Fourier transform (PFT), providing efficient image representation well adapted to image projective transformations and the retinotopic mapping of the brain visual and oculomotor pathways. Thus, the conformal camera integrates the head, eyes and retinotopy into a single computational system that allows algorithmic modeling of visual information during exploratory eye movements. In particular, we demonstrate that the image representation in terms of PFT may efficiently model the receptive fields shift that remaps cortical retinotopy in the anticipation of each saccade and the related phenomenon of perisaccadic perceptual space compression observed by human subjects in laboratory experiments (Ross et al., 1997). Notably, this system may model a new emerging role of the retina circuitry in computations of the anticipatory aspects of eye-tracking movement and a partial suppression of visual sensitivity during saccadic eye motion (Gollisch and Meister, 2010). Finally we describe our ongoing work on modeling smooth-pursuit eye movements and catch-up saccades. Relations to other work are mentioned in the last section.

2 MATHEMATICAL BACKGROUND

The conformal camera and related projective Fourier analysis were first discussed in (Turski, 2000), and later, a full mathematical formulation was presented in (Turski, 2004; Turski, 2005).

2.1 The Conformal Camera

In the conformal camera, points (x_1, x_2, x_3) of a 3D scene are projected under the mapping $j(x_1, x_2, x_3) = (x_3 + ix_1)/x_2$ into the image plane $x_2 = 1$ with complex coordinates $z = x_3 + ix_1$. The basic image transformations in the conformal camera, shown in Fig 1, are of two types.

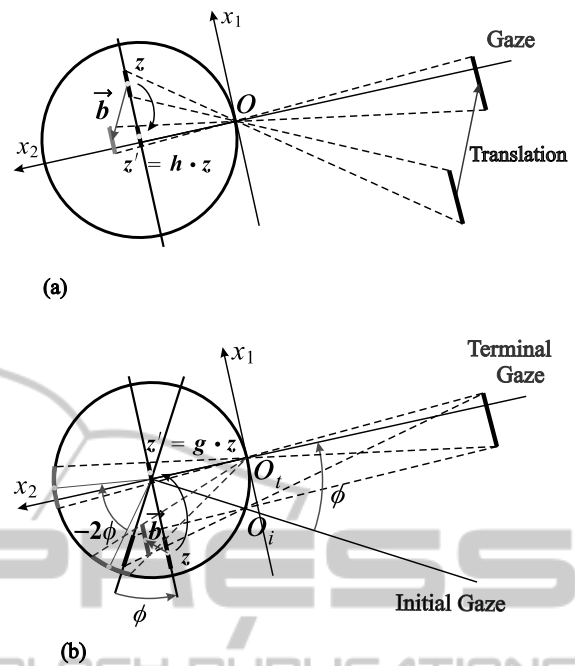


Figure 1: (a) The image transformation of a planar object translated relative to a fixed-gaze camera. (b) The image transformation resulting from the gaze change. Only 2D cross-sections are shown.

1. *The Camera Maintains a Fixed Gaze.* Image transformation resulting from a planar object's translational movement is given by the h -transformation in which an image is translated out of the image plane by $\vec{b} = (b_1, b_2, b_3)$ and then projected by j back to the image plane (Fig 1 (a)),

$$h(b_1, b_2, b_3) \cdot z = \begin{bmatrix} \delta & 0 \\ \gamma & \frac{1}{\delta} \end{bmatrix} \cdot z = \frac{1}{\delta} z + \frac{\gamma}{\delta} \quad (1)$$

where $\delta = (1 + b_2)^{1/2}$ and $\gamma = b_3 + ib_1$.

2. *The Line of Sight of the Camera is Rotated.* Image transformation of a planar stationary object is given by the hk -composition of the h -transformation (1) and the k -transformation in which an image projected by j^{-1} into the unit sphere $S_{(0,1,0)}^2$ centered at $(0, 1, 0)$ is rotated by the Euler angles (ψ, ϕ, ψ') and projected by j back to the image plane,

$$k(\psi, \phi, \psi') \cdot z = \begin{bmatrix} \bar{\alpha} & -\bar{\beta} \\ \beta & \alpha \end{bmatrix} \cdot z = \frac{\alpha z + \beta}{-\bar{\beta} z + \bar{\alpha}} \quad (2)$$

where $\alpha = e^{-i(\psi+\psi')/2} \cos(\phi/2)$ and $\beta = ie^{-i(\psi-\psi')/2} \sin(\phi/2)$. The hk -transformation is shown in Fig 1 (b). The finite iterations of (1) and (2) transformations generate (see (Turski, 2004)) the action

$$z \mapsto \begin{bmatrix} a & b \\ c & d \end{bmatrix} \cdot z = \frac{dz + c}{bz + a} \quad (3)$$

of the group

$$\mathbf{SL}(2, \mathbb{C}) = \left\{ \begin{bmatrix} a & b \\ c & d \end{bmatrix} : a, b, c, d \in \mathbb{C}, ad - bc = 1 \right\}$$

with added point at infinity ∞ such that $-a/b$ is mapped to ∞ . Thus, if $f(z)$ is the intensity function of an image, its transformations $f(g^{-1} \cdot z)$ are given by the following mappings: if $g \in \mathbf{PSL}(2, \mathbb{C})$, then

$$\begin{bmatrix} a & b \\ c & d \end{bmatrix} = g \mapsto f(g^{-1} \cdot z) = f\left(\frac{az - c}{-bz + d}\right). \quad (4)$$

We must take the quotient

$$\mathbf{PSL}(2, \mathbb{C}) = \mathbf{SL}(2, \mathbb{C}) / \{\pm Id\},$$

where Id is the identity, to identify matrices $\pm g$ because $g \cdot z = (-g) \cdot z$.

The conformal camera combines geometric and analytic (numerical) structures since $\mathbf{PSL}(2, \mathbb{C})$ is the group of holomorphic automorphisms of the Riemann sphere $\widehat{\mathbb{C}} = \mathbb{C} \cup \{\infty\}$ (Jones and Singerman, 1987) that preserves the projective geometry imposed by complex structure, known as Möbius geometry (Henle, 1997). Further, there is fully understood Fourier analysis on the group $\mathbf{PSL}(2, \mathbb{C})$ and its homogeneous spaces (Knapp, 1986).

2.2 Projective Fourier Analysis

We constructed the projective Fourier analysis by restricting geometric Fourier analysis of $\mathbf{SL}(2, \mathbb{C})$ —a direction in the representation theory of the semisimple Lie groups (Knapp, 1986)—to the image plane of the conformal camera (see Section 5.1 in (Turski, 2005)). The resulting projective Fourier transform (PFT) of a given image intensity function f is the following

$$\widehat{f}(s, k) = \frac{i}{2} \int f(z) |z|^{-is-1} \left(\frac{z}{|z|}\right)^{-k} dz d\bar{z} \quad (5)$$

where $(s, k) \in \mathbb{R} \times \mathbb{Z}$, and, if $z = x_3 + ix_1$, then $\frac{i}{2} dz d\bar{z} = dx_3 dx_1$. In log-polar coordinates (u, θ) given by $\ln re^{i\theta} = \ln r + i\theta = u + i\theta$, (5) takes on the form of the standard Fourier integral

$$\widehat{f}(s, k) = \int \int f(e^{u+i\theta}) e^u e^{-i(us+\theta k)} du d\theta. \quad (6)$$

Inverting it, we obtain the representation of the image intensity function in the (u, θ) -coordinates,

$$e^u f(u, \theta) = \frac{1}{(2\pi)^2} \sum_{k=-\infty}^{\infty} \int \widehat{f}(s, k) e^{i(us+\theta k)} ds,$$

where $f(u, \theta) = f(e^{u+i\theta})$. We stress that, although $f(e^{u+i\theta})$ and $f(u, \theta)$ are numerically equal, they are given on different spaces.

We note that in spite of logarithmic singularity of log-polar coordinates, an image f that is integrable on $\mathbb{C}^* = \mathbb{C} \setminus \{0\}$ has finite PFT

$$\begin{aligned} |\widehat{f}(s, k)| &\leq \int_0^{2\pi} \int_{-\infty}^{u_1} f(e^{u+i\theta}) e^u du d\theta \\ &= \int_0^{2\pi} \int_0^{r_1} f(re^{i\theta}) dr d\theta < \infty. \end{aligned} \quad (7)$$

This observation is crucial in constructing the discrete PFT.

2.3 Discrete Projective Fourier Transform

It follows from (7) that we can remove a disk $|z| \leq r_a$ in order to regularize f such that the support of $f(u, \theta)$ is contained within $(\ln r_a, \ln r_b) \times [0, 2\pi)$ and approximate the integral in (6) by a double Riemann sum with equally spaced partition points

$$(u_k, \theta_l) = (\ln r_a + k\delta, l\gamma), \quad (8)$$

where $0 \leq k \leq M-1$, $0 \leq l \leq N-1$, $\delta = T/M$ with $T = \ln(r_b/r_a)$, and $\gamma = 2\pi/N$. We obtain the discrete projective Fourier transform (DPFT),

$$\widehat{f}_{m,n} = \sum_{k=0}^{M-1} \sum_{l=0}^{N-1} f_{k,l} e^{u_k} e^{-i2\pi mk/M} e^{-i2\pi nl/N} \quad (9)$$

and its inverse (IDPFT),

$$f_{k,l} = \frac{1}{MN} \sum_{m=0}^{M-1} \sum_{n=0}^{N-1} \widehat{f}_{m,n} e^{-u_k} e^{i2\pi mk/M} e^{i2\pi nl/N}, \quad (10)$$

where $f_{k,l} = (2\pi T/MN) f(e^{u_k} e^{i\theta_l})$ and $\widehat{f}_{k,l} = (2\pi T/MN) \widehat{f}(u_k, \theta_l)$. Both expressions (9) and (10) can be computed efficiently by FFT.

2.4 Image Projective Transformations

Under a projective transformation by $g \in \mathbf{SL}(2, \mathbb{C})$, the retinal pixels $z_{k,l} = e^{u_k} e^{i\theta_l}$ of an image f are transformed by

$$z'_{k,l} = g^{-1} \cdot z_{k,l} = e^{u'_{k,l}} e^{i\theta'_{k,l}}.$$

For example, if the camera rotates by an angle ϕ about the vertical axis,

$$z'_{m,n} = k(0, -2\phi, 0) \cdot z_{m,n} = \frac{z_{m,n} \cos \phi - i \sin \phi}{-iz_{m,n} \sin \phi + \cos \phi}, \quad (11)$$

then the log-polar pixels (u_m, θ_n) (recall (8)) are transformed into non-uniformly spaced points $(u'_{m,n}, \theta'_{m,n})$ with the coordinates given by the equations

$$e^{2u'_{m,n}} = \frac{e^{2u_m} \cos^2 \phi + \sin^2 \phi - e^{u_m} \sin 2\phi \sin \theta_n}{e^{2u_m} \sin^2 \phi + \cos^2 \phi + e^{u_m} \sin 2\phi \sin \theta_n} \quad (12)$$

and

$$\tan \theta'_{m,n} = \frac{1/2(e^{2u_m} - 1) \sin 2\phi + e^{u_m} \sin \theta_n \cos 2\phi}{e^{u_m} \cos \theta_n}. \quad (13)$$

Computer simulations of these image projective transformations were presented in (Turski, 2003; Turski, 2005). The projectively adapted characteristics are expressed by the resulting IDPFT (see Section 9 in (Turski, 2004) for details)

$$f'_{m,n} = \frac{1}{MN} \sum_{k=0}^{M-1} \sum_{l=0}^{N-1} \hat{f}_{k,l} e^{-u'_{m,n}} e^{i2\pi u'_{m,n}k/T} e^{i\theta'_{m,n}l}, \quad (14)$$

$f'_{k,l} = (2\pi T/MN)f(u'_{k,l}, \theta'_{k,l})$. Thus, one can render image projective transformations in terms of the PFT $\hat{f}_{k,l}$ of the original image.

3 IMAGING WITH THE CONFORMAL CAMERA

The conformal camera provides a mathematical representation of visual information that efficiently supports retinal hard-wired eccentricity-dependent visual resolution and the processes of stereoscopic depth perception (Turski, 2006). In this section, we review the effectiveness of the conformal camera's non-Euclidean geometry in the intermediate-level vision problems of grouping local elements into individual objects of natural scenes and in the front-end modeling of neural mechanisms that may contribute to the continuity and stability of perisaccadic perception (Turski, 2010).

3.1 Intermediate-level Vision, Retinotopy and Peripheral Vision

Intermediate-level Vision. The image projective transformations (3) are conformal mappings with the fundamental property of mapping circles and lines either to a circle or a line (Jones and Singerman, 1987). In (Turski, 2010), we showed that these image projective transformations are relevant to the psychological and computational aspects of natural scene understanding. In fact, humans effortlessly and unambiguously group the extracted by the retina local changes in contrast representing fragmented contours (edges of occluded objects) into coherent, global shapes (intermediate-level vision). Evidence accumulated in psychological and physiological studies suggests that the human visual system utilizes a local grouping process with two simple rules: collinearity (receptive fields aligned along a line) and cocircularity (receptive fields aligned along a circle) (Sigman

et al., 2001). Further, it was suggested that cocircularity is the critical factor in the perception of texture regions (Motoyoshi and Kingdom, 2010). Now, the circles and lines are preserved under image projective transformations, thus preserving the grouping process.

Peripheral Vision. The conformal camera with its own DPFT provides an image representation computable by FFT in log-polar coordinates which simultaneously approximate retinotopy. Although the representation reduces the number of pixels more than 100 times (see Example 1 in Section 5 in (Turski, 2010)) the central region corresponding to the high-acuity foveal region has to be removed to regularize the logarithmic singularity. Without the corresponding reduction (recall discussion in Section 1), the brain would run off recourses when processing all of the incoming visual information. Further, this image representation in terms of DPFT numerically integrates both the projective image transformations produced by the conformal camera gaze changes and dependent log-polar coordinates, or retinotopic maps, providing computational framework for modeling visual information during eye movements such as saccades. It is supported by the fact that for processing visual information during saccades, only peripheral vision is important.

3.2 Processing Visual Information During Saccades

In (Turski, 2010), we developed a model, first suggested in (VanRullen, 2004), for visual information processing during saccadic eye movements. This model is based on the perisaccadic activities in which the shifts of stimuli preseaccadic receptive fields to their future postsaccadic locations is thought to underlie the scene remapping of the current foveal frame to the frame at the upcoming saccade target (Duhamel et al., 1992). This remapping uses the motor command of the impending saccade and may help maintain stability of primate perception in spite of incessant interruptions by saccades. A brief description of the model shown in Fig 2 is as follows. The eye initially fixated at **F** is starting a horizontal saccade to the target located at **T** (Fig 2, The scene). The scene with the fixation at **F** is projected into the retina (Fig 2 (a), (b)) and sampled by the photoreceptor/ganglion cells to give the set of samples $f_{m,n} = (2\pi T/MN)f(e^{u_m} e^{i\theta_n})$ (Fig 2 (c)). Next, DPFT $\hat{f}_{k,l}$ is computed by FFT in log-polar coordinates (u_k, θ_l) , where $u_k = \ln r_k$. The inverse DPFT, computed again by FFT, renders the image cortical representation $f_{m,n} = (2\pi T/MN)f(u_m, \theta_n)$. The log-polar coordinates' singularity is regularized

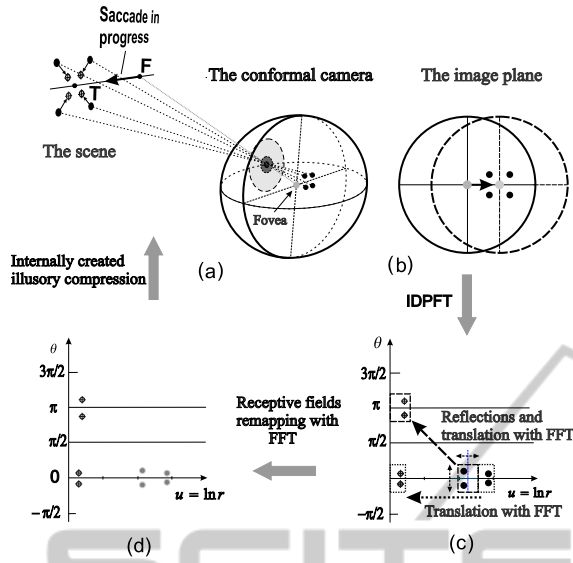


Figure 2: (a) The projection of four probes flashed around the upcoming saccade's target T in 'The scene'. (b) The probes 'retinal' images. (c) Shifts of 'cortical' receptive fields of probes using the shift property of Fourier transform. (d) Reremapped 'cortical' receptive fields. Also, the resulted probes' illusory perceptual compression referenced with arrows from the true positions are shown in 'The scene'.

by removing the (re-scaled) disk of radius 1 representing the fovea. A short time before the saccade onset and during the saccade movement redirecting the gaze line from F to T , log-polar coordinates (retinotopic maps) are remapped by shifting the frame centered at the receptive field of T to its future foveal location. This neural process is modeled by the shift properties of the inverse DPFT

$$\hat{f}_{m+h,n-j} = \frac{1}{MN} \sum_{k=0}^{M-1} \sum_{l=0}^{N-1} e^{i2\pi hk/M} e^{-i2\pi jl/N} \hat{f}_{k,l} e^{-(u_k+h\delta)} e^{i2\pi mk/M} e^{i2\pi nl/N}, \quad (15)$$

which can be computed by FFT (Fig 2 (b), (d)). We note that if the cortical image pixel $f_{m,n}$ is translated past the fovea, its translation involves both u - and θ -directions; in (15) the image is translated by h pixels in the u -coordinate and by $-j$ pixels in the θ -direction. Otherwise, it involves translation in the u -direction only, see Fig 2 (c). The perisaccadic compression observed in laboratory experiments (Ross et al., 1997) is obtained by decoding the cortical image representation to the visual field representation

$$\begin{aligned} \hat{f}_{m-h,n+j} &= (2\pi T/MN) \hat{f}(u_m+h\delta, \theta_n-j\gamma) \\ &= (2\pi T/MN) f(e^{u_m+h\delta} e^{i(\theta_n-j\gamma)}) \\ &= (2\pi T/MN) f(e^{h\delta} r_m e^{i(\theta_n-j\gamma)}), \end{aligned}$$

We see that the original position $r_m e^{i\theta_n}$ is transformed to $e^{-h\delta} r_m e^{i(\theta_n-j\gamma)}$, resulting in the compression (Fig 2, The scene).

Importantly, the shift $(-h, j)$ in terms of cortical pixels can be taken as a function of time to account for the very tight time course followed by perisaccadic compression with a duration of about 130 ms and the maximum mislocalization immediately before the saccade.

3.3 Research in Progress: Smooth Pursuit and Catch-up Saccades

During the tracking of predictably moving targets, the eyes pursuit is initially driven by the target image motion across the retina during latency. Later, when the target is almost perfectly stabilized on the fovea (zero velocity error), extraretinal mechanisms anticipating the sensory outcome of this smooth-pursuit eye movement rapidly take over and provide the neural drive to keep the eyes moving (Lisberger et al., 1987). Behavioral experiments have shown that during pursuit of unpredictable or fast moving targets, the saccadic system uses velocity error in addition to position error to generate estimates of future target position to program and trigger catch-up saccades (De Brouwer et al., 2002). Therefore, the orientation of the visual axis in space requires the coordination of smooth pursuit with catch-up saccades (Erkelens, 2006).

We assume the horizontal gaze change, given by $k(0, -2\phi, 0)$ and $\vec{b} = (b_1, b_2, 0)$, shown in Fig 1 (b). We let $g = k(0, -2\phi, 0)h(k_1, k_2, 0)$ be the composition $g = g_1 g_0$ where

$$g_0 = k(0, -2\phi_0, 0)h(b_1, b_2, 0)$$

describes an initial catch-up saccade followed by a tracking movement

$$g_1 = k(0, -2\phi_1(t), 0)h(c_1(t), c_2(t), 0).$$

We solve the equation $g = g_1 g_0$ for $h^{-1}(c_1, c_2, 0)$,

$$\begin{aligned} h^{-1}(c_1, c_2, 0) &= k(0, -2\phi_0, 0)h(b_1, b_2, 0) \\ &= h^{-1}(k_1, k_2, 0)k(0, 2\phi_0, 0), \end{aligned}$$

which has the matrix form

$$\begin{bmatrix} (1+c_2)^{-1/2} & 0 \\ -ic_1(1+c_2)^{-1/2} & (1+c_2)^{1/2} \end{bmatrix} = \begin{bmatrix} \alpha_1 & \alpha_2 \\ \alpha_3 & \alpha_4 \end{bmatrix}.$$

Then, from $\alpha_2 = 0$ we get

$$(k_2 - b_2) \cos \phi_0 = -(k_1 - b_1) \sin \phi_0, \quad (16)$$

which simplifies the other matrix elements,

$$\alpha_1 = \alpha_4^{-1} = \left(\frac{1+k_2}{1+b_2} \right)^{1/2} = (1+c_2)^{-1/2}$$

$$\alpha_3 = -i \left(\frac{k_1 - b_1}{1 + b_2} \right) \left(\frac{1 + k_2}{1 + b_2} \right)^{-1/2} = -ic_1(1 + c_2)^{-1/2}.$$

Now α_1 , α_3 and (16) lead to the relations between the vectors $\vec{c} = (c_1, c_2, 0)$, $\vec{b} = (b_1, b_2, 0)$, and $\vec{k} = (k_1, k_2, 0)$ and the angle ϕ_0 summarized in Table 1.

Table 1: All solutions of the composition of two gaze-changes. Here, + or - means that the value of the quantity in this column is positive or negative, respectively. the other choices of + or - results in contradictions.

$1 + b_2$	$1 + c_2$	$1 + k_2$	
+	+	+	$k_1 = \frac{b_1 + c_1 + b_1 c_2 + c_1 b_2}{1 + c_2}$, $k_2 = \frac{b_2 - c_2}{1 + c_2}$, $c_2 = c_1 \tan \phi_0$
-	+	-	$k_1 = \frac{b_1 + c_1 + b_1 c_2 + c_1 b_2}{1 + c_2}$, $k_2 = \frac{b_2 - c_2}{1 + c_2}$, $c_2 = c_1 \tan \phi_0$
-	-	+	$k_1 = \frac{b_1 - c_1 + b_1 c_2 - c_1 b_2}{1 + c_2}$, $k_2 = \frac{b_2 - c_2}{1 + c_2}$, $c_2 = -c_1 \tan \phi_0$

Here the saccadic gaze rotation problem is different than the one discussed in Section 3.2 since the target is moving. We show that the vector parameters of the smooth pursuit \vec{c} are linked to the saccadic eye rotation ϕ_0 . Since the smooth pursuit rotation angle $\phi_1(t)$ can be considered known (efference copy or anticipatory mechanisms), only one internal parameter $c_1(t)$ is needed to describe the retinal image transformation during the smooth-pursuit movement of the conformal camera. Thus, the results we present in this section should support the fact that smooth pursuit and saccades are not independent (Erkelens, 2006). We intend to use the compositions of gaze changes we presented in this section to model the eye movement sequences, see (Quaia et al., 2010) for example.

4 CONCLUSIONS

The conformal camera provides a computational framework that has the unique capability of developing algorithms for processing visual information during the exploratory motion of a camera with anthropomorphic visual sensors that resemble a sequence of saccades interlaced with fixations. In particular, we presented algorithmic steps based on the front-end neural processes of the perisaccadic perception that are using the oculomotor command of the impending saccade to shift stimuli receptive fields in cortical areas to their future postsaccadic locations. This shift is thought to underlie the scene remapping of the current foveal frame to the frame at the upcoming saccade target and may help acquire the visual information without repeating, afresh, the whole process at each fixation and maintain stability of primate perception in spite of about 200,000 saccades produced each day. Because the shift occurs in log-polar coordinates, it explains perisaccadic spatial distortion. Also, the

conformal camera seems to be able to model smooth-pursuit eye movements, as our preliminary results are suggesting. Of course, much more work has to be done before the system could be tested.

In addition to our model of perisaccadic perception (Section 3.2), there is one another elaborate computational modeling that assumes that the flashed stimuli receptive fields in cortical areas dynamically change position toward the saccade target receptive field as the result of the gain of feedback of the retinotopically organized activity hill of the saccade target in the oculomotor superior colliculus layer (Hamker et al., 2008). The perceived spatial distortion of stimuli is the result of the cortical magnification factor of the retinotopic mapping when the position of each stimulus is decoded from activity of the neural ensemble. What sets apart our modeling from the other model is the fact that the computational efficiency is built into the modeling process (computations with FFT) and it accommodates other types of eye movements. In the case of saccadic eye movement, this is especially important because the occurrence of three saccades per second and the time needed for the oculomotor system to plan and execute each saccade.

REFERENCES

- de Brouwer S, Yuksel D, Blohm G, Missal M, and Lefevre P. (2002). What triggers catch-up saccades during visual tracking? *Journal of Neurophysiology*, 87, 1646-1650.
- Duhamel J-R, Colby C. L, and Goldberg M. E. (1992). The updating of the representation of visual space in parietal cortex by intended eye movements, *Science* 255, 90-92.
- Erkelens C J. (2006). Coordination of smooth pursuit and saccades, *Vision Research*, 46, 163-170.
- Gollisch T and Meister M. (2010). Eye Smarter than Scientists Believed: Neural Computations in Circuits of the Retina, *Neuron*, 65, 150-164.
- Hamker F. H, Zirnsak M, Calow D, and Lappe M. (2008). The Peri-Saccadic Perception of Objects and Space, *PLoS Computational Biology* 4(2):e31. doi:10.1371/journal.pcbi.0040031.
- Henle M. (1997). Modern Geometries. The Analytical Approach, *Prentice Hall*, Upper Saddle River, NJ.
- Jones G and Singerman D. (1987). Complex Functions, *Cambridge University Press*, Cambridge.
- Klier E. M. and Angelaki D. E. (2008). Spatial Updating and the Maintenance of Visual Constancy, *Neuroscience* 156, 801-818.
- Knapp A. W. (1986). Representation Theory of Semisimple Groups: An overview Based on Examples, *Princeton University Press*, Princeton, NJ.

- Lisberger S. G., Morris E. J., and Tychsen L. (1987). Visual motion processing and sensory-motor integration for smooth pursuit eye movements, *Annual Review Neuroscience*, 10, 97-129.
- Melcher D. and Colby C. L. (2007). Trans-saccadic perception, *Trends in Cognitive Sciences*, 12, 466-473.
- Motoyoshi I. and Kingdom F. A. (2010). The role of cocircularity of local elements in texture perception, *Journal of Vision* 10(1):3, 1-8.
- Quaia C., Joiner W. M., Fitzgibbon W. J., Optican L. M., and Smith M. A. (2010). Eye movement sequences generation in humans: Motor or goal updating? *Journal of Vision*, 10(14):28, 1-31.
- Ross, J., Morrone M C, and Burr D C. (1997). Compression of visual space before saccades, *Nature*, 386, 698-601.
- Sigman M, Cecchi G A, Gilbert C. D., and Magnasco M. (2001). On a common circle: Natural scenes and Gestalt rules, *Proceedings of the National Academy of Sciences of the U.S.A.*, 98, 1935-1940.
- Turski J. (2000). Projective Fourier analysis for patterns, *Pattern Recognition*, 33, 2033-2043.
- Turski J. (2004). Geometric Fourier Analysis of the Conformal Camera for Active Vision, *SIAM Review*, 46, 230-255.
- Turski J. (2005). Geometric Fourier Analysis for Computational Vision, *Journal of Fourier Analysis and Applications*, 11, 1-23.
- Turski J. (2006). Computational Harmonic Analysis for Human and Robotic Vision Systems, *Neurocomputing*, 69, 1277-1280.
- Turski J. (2010). Robotic Vision with the Conformal Camera: Modeling Perisaccadic Perception, *Journal of Robotics*, doi:10.1155/2010/130285, 1-16.
- VanRullen R. (2004). A simple translation in cortical log-coordinates may account for the pattern of saccadic localization errors, *Biological Cybernetics*, 91, 131-137.
- Wurtz R. H. (2008). Neural mechanisms of visual stability, *Vision Research*, 48,2070-2089.